Nanocomposites of TiO_2/Cyanoethylated Cellulose with Ultra High Dielectric Constants

Nadeesh Madusanka,[1] Sai G. Shivareddy,[1] Pritesh Hiralal,[1] Mark D. Eddleston,[2] Youngjin Choi[1], Rachel A. Oliver[3] and Gehan A J Amaratunga [1]*

[1] Department of Engineering, University of Cambridge, 9 JJ Thomson Avenue, Cambridge CB3 0FA, United Kingdom
Email: gaja1@cam.ac.uk, Fax: +44 (0)1223 748348; Tel: +44 (0)1223 748325
[2] Department of Chemistry, University of Cambridge, Lensfield Road, Cambridge, CB2 1EW. United Kingdom
[3] Department of Materials Science and Metallurgy, University of Cambridge, 27 Charles Babbage Road, Cambridge, CB3 0FS, United Kingdom

Abstract

A novel dielectric nanocomposite containing a high permittivity polymer, cyanoethylated cellulose (CRS) and TiO_2 nanoparticles was successfully prepared with different weight percentages (10%, 20% and 30%) of TiO_2. The intermolecular interactions and morphology within the polymer nanocomposites were analysed. TiO_2/CRS nanofilms on SiO_2/Si wafers were used to form metal-insulator-metal (MIM) type capacitors. Capacitances and loss factors in the frequency range of 1 kHz to 1 MHz were measured. At 1 kHz CRS-TiO_2 nanocomposites exhibited ultra high dielectric constants of 118, 176 and 207 for nanocomposites with 10%, 20% and 30% weight of TiO_2 respectively, significantly higher than reported values of pure CRS (21), TiO_2 (41) and other dielectric polymer-TiO_2 nanocomposite films. Furthermore, all three CRS-TiO_2 nanocomposites show a loss factor < 0.3 at 1 kHz and low leakage current densities (10^{-6} A/cm^2-10^{-7} A/cm^{-2}). Leakage was studied using conductive atomic force microscopy (C-AFM) and it was observed that the leakage is associated with TiO_2 nanoparticles embedded in the CRS polymer matrix. A new class of ultra high dielectric constant hybrids using nanoscale inorganic dielectrics dispersed in a high permittivity polymer suitable for energy management applications is reported.

Keywords: nanocomposites, ultrahigh dielectric constants, thin films, C-AFM

Introduction

Energy management is a key requirement for portable/mobile electronic and electrical systems. The mobility of a product/system and its range/operational time between electrical charging is crucially dependent on the specific energy density of the energy storage devices (batteries and capacitors) [1]. In addition there is a requirement for high power density to meet burst energy demand. Dielectric capacitors are one of the potential energy management

devices, having very high power densities, which can provide energy bursts of high current within a very short period of time; however, they have relatively low energy densities [2]. Nanomaterial based dielectrics are promising candidates to meet the required technological demand in dielectric ultra capacitors for energy management applications as well as for miniaturising power electronics where energy ballasting using capacitors is essential [3]. Organic/Inorganic nanocomposites have received much attention in the formulation of novel high permittivity dielectrics as they exhibit unique properties compared to conventional composite materials [4-10]. TiO_2 is a versatile material used in a range of applications including nanodielectrics where composites of nanoscale TiO_2 with different polymers form the dielectric. The first dielectric nanocomposite based on TiO_2 nanoparticle and polystyrene was reported by Bandyopadhyay et al in 1988 [11]. Subsequently, in 1994 Lewis reported a landmark theoretical study on dielectric nanocomposites [12]. However, this theoretical work only became widely recognised after publication of the experimental study by Nelson et al in 2002 on a dielectric nanocomposite based on TiO_2 nanoparticles and epoxy resin (k=8.5 at 1 kHz for 500-750 ε m thick films) [13]. In 2004, Cheng et al reported a dielectric nanocomposite (k=7.5 at 50 kHz) of cross linked poly-4-vinylphenol and TiO_2 nanoparticles deposited by spin coating techniques [14]. In addition, Nelson et al studied the internal charge behaviour of TiO_2-epoxy nanocomposites using dielectric spectroscopy, electroluminescence and thermally stimulated current and photoluminescence [3]. The synthesis of organic-inorganic core shell nanoparticles using TiO_2 as the core nanoparticle and polystyrene as the shell has been reported by Maliakal et al[16] and they observed a dielectric constant enhancement of over 3 times that of bulk polystyrene for 1.25 ε m thick films at 1kHz [15]. Nanocomposites of polypyrrole/TiO_2 (k=140 at 1 kHz for 0.5 mm thick films) and PMMA/TiO_2 (k= 25 at 1 kHz for 5 mm thick films) have been reported previously [16, 17]. The dielectric behaviour of nanocomposites based on ferroelectric poly(vinylidenefluoride-*ter*-trifluoroethylene) and poly (vinylidenefluoride-*ter*-trifluoroethylene-*ter*-chlorotrifluoroethylene) with TiO_2 nanoparticles (k= 12 and 42 respectively at 1kHz for 25-50 ε m thick films) were also examined by Li et al [18]. In addition, nanocomposites of TiO_2-poly(vinylidenefluoride) [19], TiO_2- poly(4-vinylphenol) [20] and TiO_2-polyimide [21] have been recently reported in the literature. The existing literature on dielectric polymer nanocomposites containing TiO_2 report dielectric constants from low as 5 to 140 at best. Additionally, in most of the cases; film thickness was in the micrometer to millimetre range, which is unsuitable for achieving high capacitance in the 3 ï 24V range typical for mobile

electronic systems. Here, we report ultra high dielectric constants (> 200) in thin films (100-150 nm) of high permittivity polymer nanocomposites.

A novel dielectric nanocomposite comprising a high permittivity polymer, cyanoethylated cellulose (CRS) with different weight percentages (10%, 20% and 30%) of TiO_2 nanoparticles is reported. CRS is a cyanoresin which contains CO and CN dipoles which are responsible for dielectric behavior and due to the polar nature of the polymer matrix it shows a strong affinity for inorganic oxides [22]. The molecular structure of CRS polymer is shown in figure 1(a). Nanocomposites of CRS with nanoscale dielectrics have not been studied previously and TiO_2, which possesses a higher dielectric constant and larger band gap yields significantly, enhanced dielectric properties. Schematic representation of a metal-insulator-metal (MIM) type capacitor with a TiO2-CRS dielectric film is shown in figure 1(b) below.

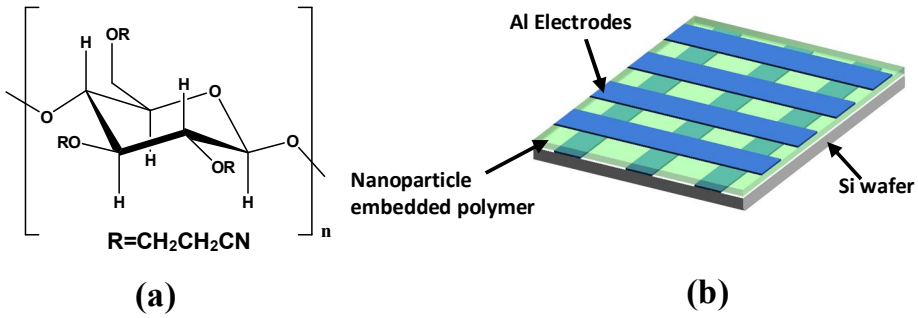

Figure 1 (a) Molecular structure of CRS and (b) schematic illustration of a MIM capacitor

Experimental

Materials

TiO_2 anatase nanoparticles and acetone were purchased from Sigma Aldrich, USA and CRS polymer were purchased from Shin-Etsu Chemical Co. Ltd. Japan. All chemicals were used without further purification.

Preparation of films of CRS-TiO_2 nanocomposite

CRS polymer was dissolved in acetone to prepare a polymer solution (20 gdm^{-3}) and different volumes of polymer solution were mixed with TiO_2 nanoparticles (25 nm) and stirred for 24 hours to obtain TiO_2/CRS dispersions with different TiO_2 weight percentages; 10 % (3.45 vol%), 20 % (6.65 vol%) and 30 % (9.65 vol%) respectively. Spin coating of CRS-TiO_2 dispersions at 2500 rpm for 20s was the method used to deposit polymer nanocomposite films on clean n-type Si wafer (with 200 nm SiO_2 layer) and this was followed by thermal annealing at 150 ^oC for 3 hours.

Characterisation CRS-TiO_2 nanocomposite

PXRD data of the dielectric films were collected on a Phillips PW3710 diffractometer with nickel-filtered CuKŬ radiation (1.5406 Å) using a scanning RTMS XôCelerator detector. The morphology and film thickness were analysed by Scanning Electron Microscopy (SEM) using a HITACHI SS5500 microscope. Conductive atomic force microscopy (C-AFM) was carried out on a Veeco Dimension 3100 atomic force microscope (AFM) using a commercially-available extended tunneling atomic force microscopy (extended-TUNA) module. Platinum-iridium coated probes (from Veeco, model: SCM-PIC) were used. X-ray photoelectron spectroscopy (XPS) was carried out using a ESCALAB 250 Xi equipped with a monochromatic Al KŬ X-ray source in a ultrahigh vacuum. Ultra-violet photoemission spectroscopy (UPS) was also carried out using a ESCALAB 250 Xi with a UV excitation source of He-I emission at 21.21 eV in a ultrahigh vacuum. Fourier transform infra-red spectroscopy was performed using a Bruker Vertex80 in the range from 600 to 4000 cm^{-1} using the attenuated total reflectance technique. Thermogravimetric analysis (TGA) was carried out using a Mettler Toledo TGA/SDTA851e/SF/1100 instrument with an air purge flow rate of 50- 70 cm^3min^{-1} (ramp 10^oC/min).

Fabrication of metal-insulator-metal (MIM) type capacitors

CRS- TiO_2 nanofilms on SiO_2/Si wafers were used to form metal-insulator-metal (MIM) type capacitors (100 nm Al layers deposited by thermal evaporation were used as metal top and bottom electrodes). Capacitance measurements of the nanocomposites over a range of frequencies from 1 kHz to 1 MHz, capacitance-voltage measurements and current-voltage measurements were performed on a Microtech cascade probe station.

Results and Discussion

The PXRD traces of the prepared CRS-TiO_2 nanocomposites, commercial samples of TiO_2 and CRS polymer are given in figure 2. The peak positions of the TiO_2 sample are consistent with the anatase phase of TiO_2. It was observed that the PXRD pattern of the TiO_2 in the composite has no obvious difference with pristine TiO_2 which indicates that the crystal structure of TiO_2 is unchanged when it is incorporated into a CRS polymer matrix. In the PXRD pattern of CRS polymer, the amorphous nature of the polymer is indicated by the broad peaks at around 10^o and 20^o 2ɗ. A similar feature was observed for the CRS matrix of the composite.

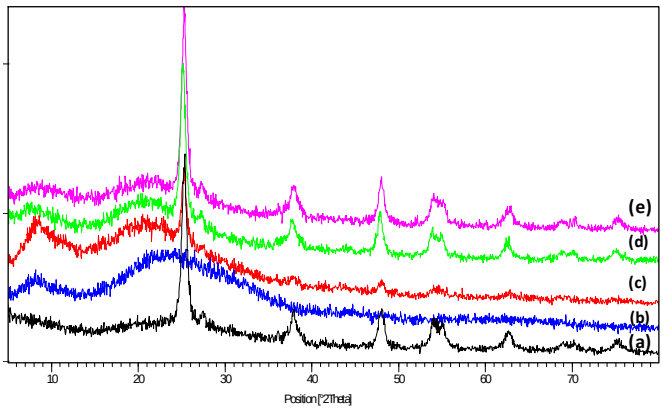

Figure 2 PXRD traces of (a) Pristine TiO_2 (b) CRS polymer (c) CRS-TiO_2 10% (d) CRS-TiO_2 20% (e) CRS-TiO_2 30%

Furthermore, there is no evidence of impurity phases in the prepared composite and the intensities of peaks corresponding to the anatase phase of TiO_2 increase with the loading of TiO_2.The morphology of the nanocomposites was studied using scanning electron microscopy and is shown in figure 3.

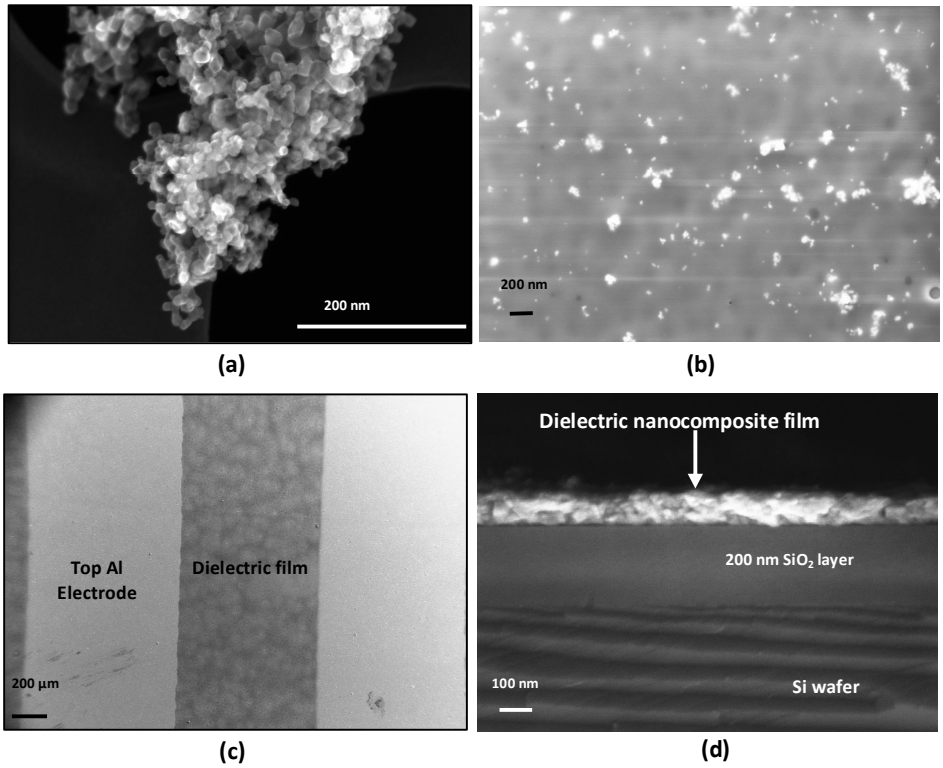

Figure 3 SEM images of (a) TiO_2 nanoparticles (b) surface view of a CRS-TiO_2 nanocomposite (10% TiO_2) (c) top view of the MIM capacitor (d) cross section of a CRS-TiO_2 (10% TiO_2) nanofilm

It is seen that the TiO_2 nanoparticles are distributed in the polymer matrix and the size and shape of the TiO_2 nanoparticles remain unchanged. However, the CRS polymer matrix is highly sensitive to the electron beam which cause melting during imaging. Fig. 3(c) shows the appearance of the top contact (100 nm Al layer) on the polymer film and Fig. 3(d) shows a cross section of a CRS-TiO_2 thin film on a SiO_2 200nm/Si wafer. It was observed that the average film thickness for the 10% weight TiO_2 polymer film was about 85 nm, 110 nm with 20% weight TiO_2 and 120 nm with 30% weight TiO_2. The film thicknesses of the 10% and 20% weight TiO_2 polymer films are more uniform, smooth and dense in comparison with the 30% weight TiO_2 polymer film, TiO_2 nanoparticle aggregation is clearly evident in the film with to the highest 30% loading of nanoparticles (supplementary information S2).

X-ray photoelectron spectroscopy was employed to study the interaction between the CRS polymer and TiO_2 nanoparticles. The N 1s peak from the bare CRS polymer and CRS-TiO_2 and Ti 2p peak from bare TiO_2 and CRS-TiO_2 are shown in figure 4.

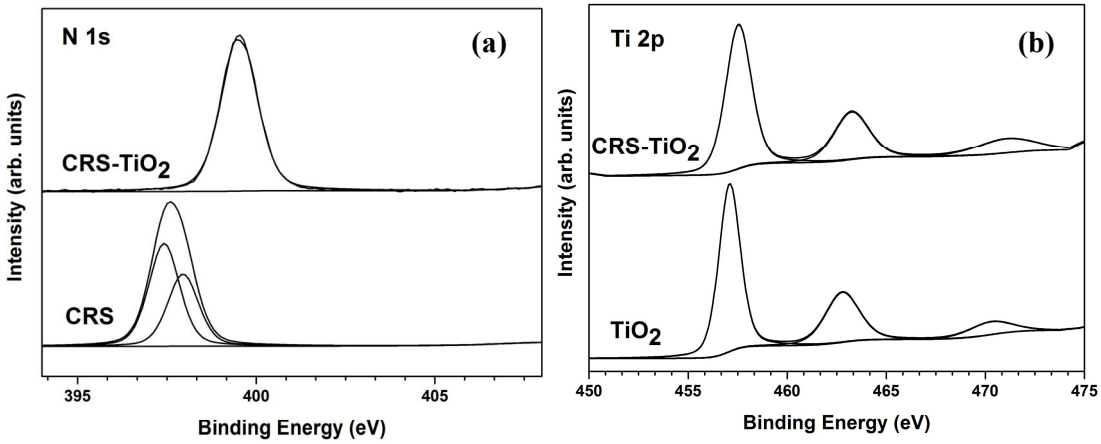

Figure 4 XPS (a) N1s spectra for CRS and CRS-TiO_2 (10%) nanocomposite and (b) Ti2p spectra for TiO_2 and CRS-TiO_2 (10%) nanocomposite

The N1s spectra for the CRS polymer showed two major peaks with binding energies of 397.4 eV and 397.9 eV. However, N1s spectra for the CRS-TiO_2 showed only a single peak at 399.1 eV. The shifting of the binding energy of N1s in the CN group of the polymer confirms the interaction of the CRS polymer with TiO_2 nanoparticles. Furthermore, the Ti2p XPS spectra shows two main peaks at 457.2 eV and 462.8 eV due to the spin-orbit pairs of $2p^{3/2}$ and $2p^{1/2}$. In addition, a satellite peak at 470.4 eV was observed [23]. Similar trend was observed for the Ti 2p in CRS-TiO2 ($2p^{3/2}$ peak at 457.6 eV, $2p^{1/2}$ peak at 463.3 eV and satellite peak at 471.3 eV) and significant changes in the binding was not observed. A notable change in the binding energies of C1s and O1s were not observed.

FTIR spectra of TiO_2, CRS polymer and CRS-TiO_2 nanocomposite were recorded (Supplementary Information S1). TiO_2 shows absorption bands at 3350 cm^{-1}, 1630 cm^{-1} and 734 cm^{-1} due to O-H stretching, O-H bending of surface adsorbed water and the Ti-O stretching mode of TiO_2 respectively. CRS polymer shows broad O-H stretching band around 3400 cm^{-1} and an O-H bending mode at 1625 cm^{-1} due to OH groups present in the polymer. In addition, CN stretching band appears at 2252 cm^{-1} and peaks at 2900 cm^{-1} and 1050 cm^{-1} correspond to CH_2 stretching and bonding modes. It was observed that the CN stretching vibration mode of the CRS polymer has been slightly shifted to a lower wave number from 2252 cm^{-1} to 2243 cm^{-1} in the CRS-TiO_2 composite which indicate interactions of the CN group with the Ti (IV) metal centre. Furthermore, Ti-O groups in TiO_2 can also interact with O-H groups present in the polymer.

TGA analysis of CRS polymer and TiO_2-CRS nanocomposite are shown in figure 5. A major weight loss in the range of 250 ^oC and 400 ^oC was observed with a large slope which is attributed to the random internal scission of CRS polymer chains. As shown in the DTA curve, onset degradation temperatures of the bare CRS polymer and CRS chemically attached to TiO_2 nanoparticles are 274 ^oC and 282 ^oC respectively. This thermal stability enhancement further confirms interaction between TiO_2 nanoparticles and the polymer matrix. However, TiO_2-CRS nanocomposite degrades rapidly after the onset degradation temperature compared to the bare CRS polymer.

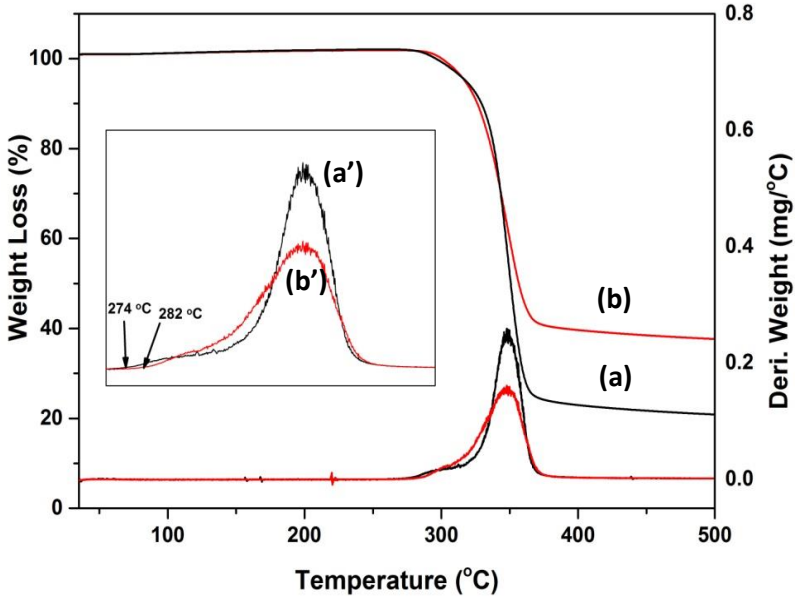

Figure 5 TGA curve (a) and DTA trace (a') for CRS polymer and TGA curve (b) and DTA trace (b') for 10% CRS-TiO_2 nanocomposites

UV absorption spectra of TiO_2, CRS polymer and CRS-TiO_2 nanocomposites were recorded and are shown in figure 6. In the case of TiO_2, the UV absorption is explained using band theory. TiO_2 has a relatively large band gap of 3.2 eV. CRS polymer shows a UV absorption band around 300 nm due to the presence of CN groups in the polymer.

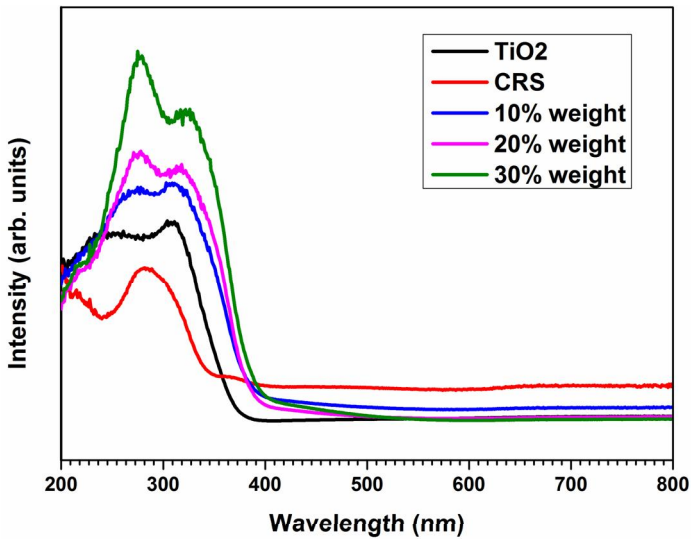

Figure 6 UV/Vis spectra for TiO_2, CRS and CRS-TiO_2

It is observed that the UV band of the CRS polymer has blue shifted in the composite while a slight red shift is seen for the TiO_2 UV band which provides further evidence of interaction between TiO_2 nanoparticles and the CRS polymer matrix.

The capacitances of the CRS-TiO_2 nanocomposite films and bare CRS polymer were measured in the frequency range from 1 kHz to 1 MHz and are shown together with their respective dielectric constants in figure 6. Capacitance (C) is a quantity which gives how much electric charge can be stored in a capacitor. The fundamental equation, $C= \varepsilon_o\varepsilon_r A/d$ of a parallel plate capacitor where ε_o is the dielectric constant of the free space (8.854×10^{-12} F/m), ε_r is the dielectric constant of the dielectric layer, A is the effective area of the dielectric film and d is the thickness. Using the geometric parameters in the equation for C the equivalent dielectric constant of the nanocomposites can be calculated. The capacitance values for all three composites remain virtually constant up to 500 kHz and then sharply decreases with increasing frequency (Fig. 7(a)). At low frequencies dipoles follow the field and as the frequency increases dipoles response starts to lag behind the field and dielectric constant/capacitance slightly decreases. When the frequency reaches 0.8 ï 1 MHz dielectric constant/capacitance drops due to the interfacial polarisation states between the TiO_2

nanoparticles and CRS polymer interface not being able to respond/follow the field. It appears as an apparent relaxation of the polarized states [24] and the capacitance drops to the baseline of the CRS polymer without the TiO_2 nanoparticles. The obtained capacitance values depend on the thickness of the film. Dielectric constants for all three composites were calculated using the average film thickness measured by AFM (Supplementary Information S2) (Fig. 7(b)). At 1 kHz CRS- TiO_2 nanocomposites exhibited ultra high dielectric constants of 118, 176 and 207 with 10%, 20% and 30% weight of TiO_2 respectively which is significantly higher than of pure CRS (21) [7], close to the value of 25 measured here (Fig. 7(b)) and reported value for TiO_2 (41) [25] films.

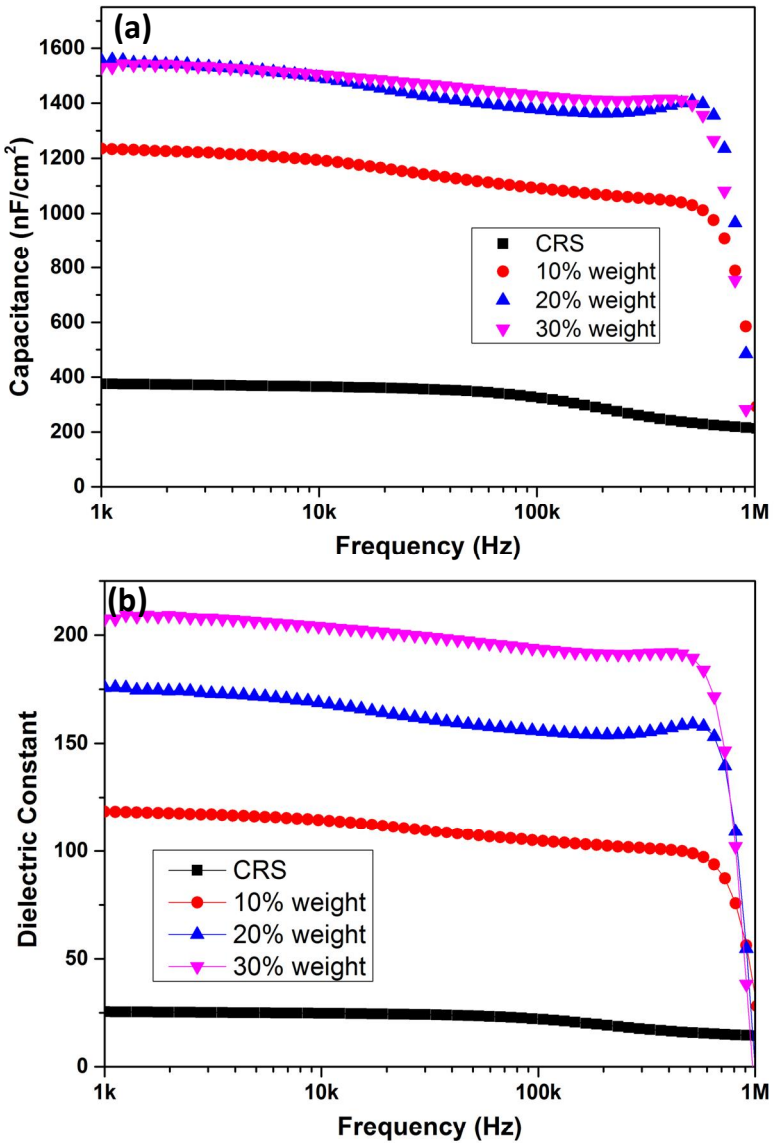

Figure 7 (a) Capacitance and (b) dielectric constant as a function of frequency for CRS-TiO_2 nanocomposites with different TiO_2 loadings.

Furthermore, all three CRS-TiO_2 nanocomposites show a loss factor < 0.3 at 1 kHz (Supplementary Information S3) and low leakage current densities.

Fig. 8 (a) shows capacitance-voltage measurements for all three nanocomposite films and bare CRS polymer, which provides information about the charge behaviour of the dielectric films. In general, it was observed that capacitance values for all three nanocomposites and bare CRS polymer in the voltage range of -2V to 2V are stable. However, when voltage varies around 0V (either negative or positive), capacitance of 30% weight nanocomposite gradually increases whereas; an initial increase is followed by a gradual decrease for the 10% weight nanocomposite. This type of variations may be due the charging of TiO_2-CRS interface and nanocomposite film Al electrode interface. Fig. 8 (b) shows the current density-voltage curves for bare CRS polymer and CRS-TiO_2 nanocomposite films with different TiO_2 loadings.

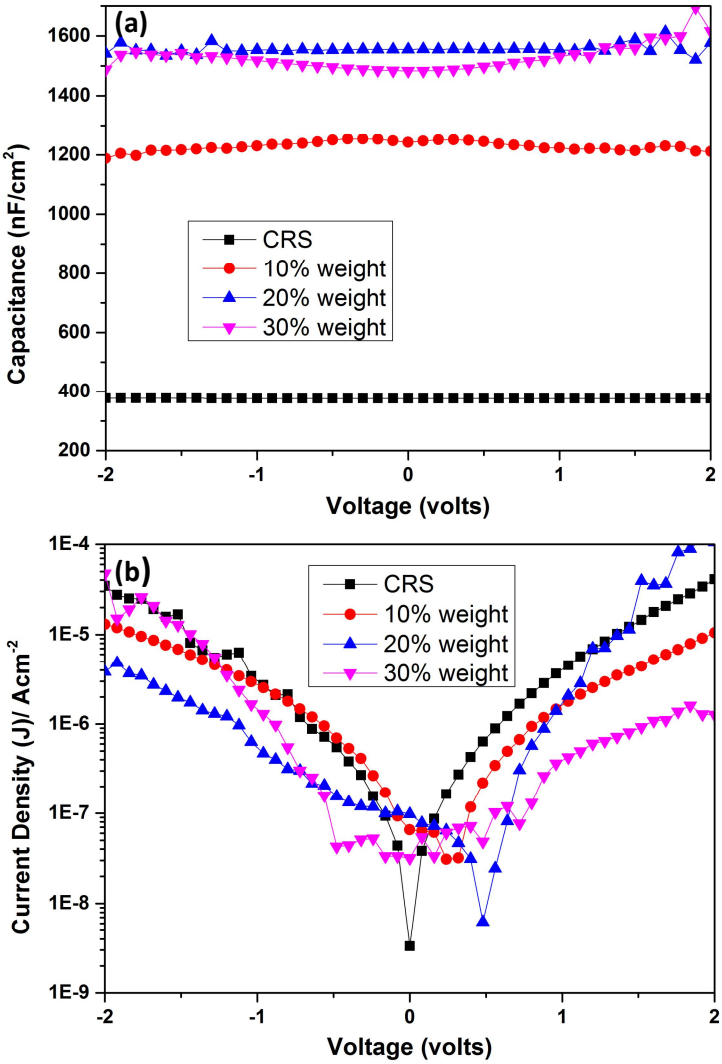

Figure 8 Capacitance (a) and current densities (b) as a function of voltage for CRS-TiO_2 nanocomposites with different TiO_2 loading

The leakage current densities are relatively low, in the range of 10^{-6} A/cm^2-10^{-7} A/cm^{-2} which is indicative of a dense chemical structure in the nanocomposite. However, current voltage characteristics possess a distinct asymmetry and a minimum is observed around 0.5V for all three composites with different TiO_2 loading. This shift in the minimum current from 0V could be due to the charging of the TiO_2-CRS interfaces.

Figure 9 shows AFM images of CRS-TiO_2 nanocomposite films which give further information about their surface morphology and current distribution. It can be seen that TiO_2 nanoparticles are embedded in the polymer matrix and coated with the polymer. The presence of nanoparticles within the polymer give arises to topology differences in the AFM topography image as shown in figure 9(a) (lighter regions). The bright spots in the topography image are thought to originate from TiO_2 nanoparticles exposed on the surface. It was observed that the nanocomposite films are dense and pinhole free resulting in reduced the leakage current through the dielectric layer. The corresponding current distribution image of CRS-TiO_2 nanocomposite is shown in figure 9(b).

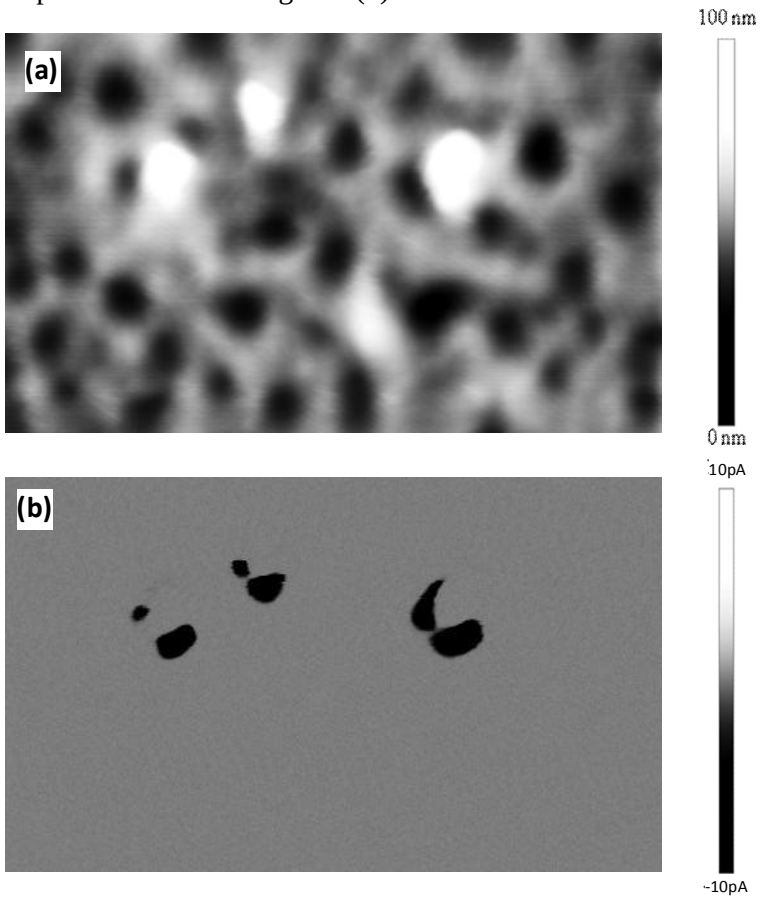

Figure 9 AFM (a) topography and (b) current distribution image of CRS-TiO_2 10% nanocomposite

In the C-AFM configuration used, the applied biasing conditions, negative currents are measured, corresponding to dark spots in the C-AFM image. The dark spots in the current image are in the vicinity of three of the TiO_2 particles, although it is not clear at this stage whether the distinctive double-lobed shape of the current spots is a tip-induced artefact or a real effect. Nonetheless, leakage paths through the nanocomposite appear to be associated with the TiO_2 nanoparticles

According to the logarithmic mixing rule [7], the highest dielectric constant which can be achieved by a composite is found to be below the dielectric constant of the filler. However, in the case of nanoscale fillers with high permittivity polymers, significantly high dielectric properties have been achieved [16]. It has been reported that the interface between the nanoscale filler and the polymer plays the major role, and a model termed The Interface Model has been proposed to for the interface zone between the nanoparticle and the polymer [26, 27]. According to this model, properties of the polymer chains combined with nanoparticles differ from the properties of the more distant polymer chains. As a consequence, it is proposed the interface zone between the nanoparticle and polymer has a significant influence on the properties of the dielectric as a whole. The interfacial region surrounding nanoparticles in the nanocomposite is dominant due to the high surface to volume ratio, whereas, it is insignificant for bulk fillers. Therefore properties of the resulting nanocomposite more resemble the interface zones rather than those of the original constituents. Schematic representations of Interface Model and a nanoparticles embedded polymer matrix of CRS-TiO_2 nanocomposite are shown in figure 10.

According to Tanaka et al [26], dielectric nanoparticles dispersed in a polymer matrix result in the formation of different layers; a bound layer and a loose layer. The first layer corresponds to the nanoparticle and polymer bonding through functional groups to form an interface. If the polymer contains a significant amount of mobile ionic charge, a diffuse electrical double layer is formed. If the polymer does not contain ionic species dipole orientation is generated from an applied electric field. The second layer consists of polymer chains strongly bonded to the first layer. The third layer is a region of polymer loosely bound to the second layer. It is believed that such polarisation phenomena occurring in the interface zones of nanoparticles are responsible for ultra high dielectric constants measured in these dielectric nanocomposites. In the current system CRS polymer which carries polar CN and CO groups interact with the TiO_2 nanoparticles forming a polarized double layer in the polymer nanoparticle interface resulting in enhanced dielectric properties.

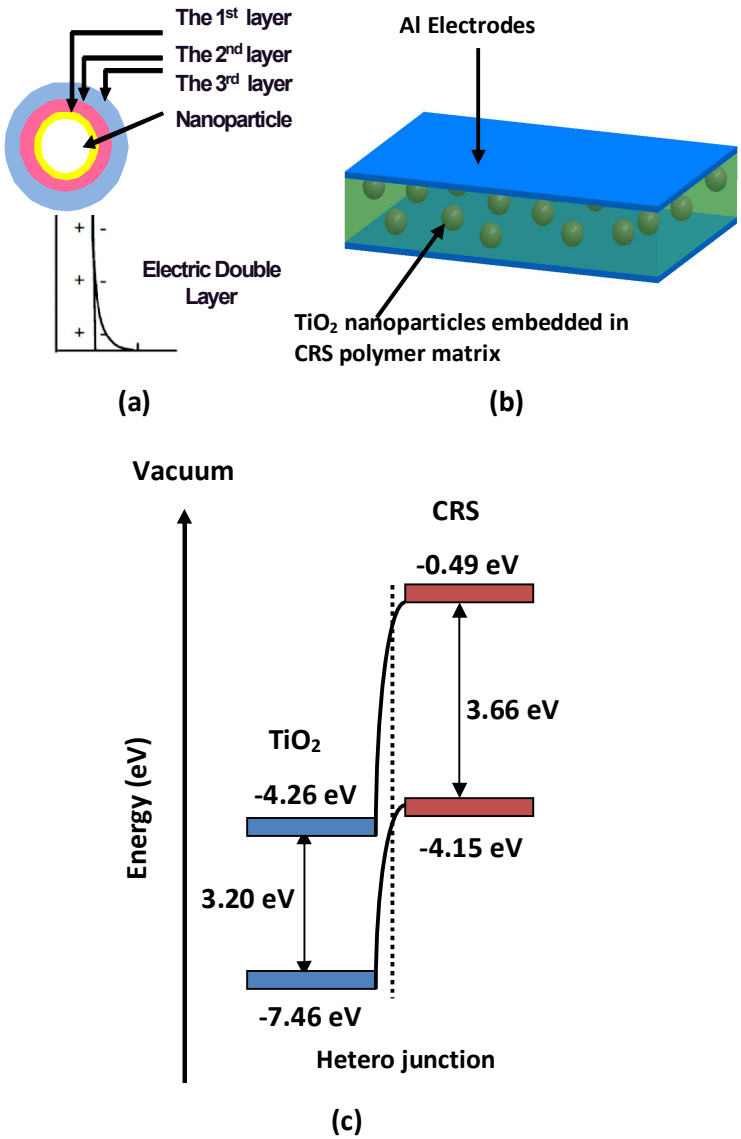

Figure 10 Schematic representation of (a) the Interface Model (b) nanoparticles embedded polymer matrix of CRS-TiO_2 nanocomposite and (c) energy bands of CRS-TiO_2 nanocomposite

However, dielectric property enhancement is a cumulative effect of the intrinsic properties of the inorganic filler (dielectric properties, nanoscale particle size etc) and the polymer (dielectric properties, network forming capability etc) and specially the types of interactions between two components and the nature of the interface. In figure 10 (c) the CRS polymer HOMO and LUMO energy levels (extracted using UV/Vis and UPS data, see supplementary information S4 and S5 respectively. It is worth noting that this is the first report of these levels for CRS) are aligned to those of TiO_2. As seen from Fig. 10(c) the energy level

alignments are such that TiO_2 can act as an acceptor of electrons from the HOMO level of CRS in to its conduction band/LUMO level. This gives insight into why the interface/junction between TiO_2 and CRS can become charged to give nanoscale electrical double layers which are distributed through the dielectric. Though interface polarisation between the TiO_2 and the CRS can take place due to their different dielectric constants and conductivities, the shifts seen in the XPS, TGA and FTIR data, indicate a form of weak non covalent hydrogen-like bonding aids the polarisation through a charge transfer process. The charge transfer from the polymer to the TiO_2 (or vice-versa) will depend on the HOMO and LUMO energy levels of the polymer. CRS is particularly suited for this and hence gives rise to the ultra-high dielectric constants seen where in a composite with TiO_2 nanoparticles.

Conclusions

CRS-TiO_2 nanocomposites which exhibit ultra high dielectric constants (Ɛr) of 118, 176 and 207 with 10%, 20% and 30% weight of TiO_2 are presented. The reported Ɛr values of the nanocomposite are significantly higher than reported values for pure CRS (21) and TiO_2 (41) films. All three CRS-TiO_2 nanocomposites show a loss factor < 0.3 and low leakage current densities. C-AFM results indicate that leakage current is associated with regions around which TiO_2 nanoparticles are embedded in the polymer matrix. It is hypothesised that the polymer-nanoparticle interface plays a major role in enhancing the dielectric properties of the nanocomposite as per the Interface Model [26, 27]. The enhanced leakage which is seen around the nanoparticles could be indicative of the higher charge densities in the interface region. We show that the HOMO-LUMO energy alignments between CRS and TiO_2 are indeed favourable for enabling charge transfer and polarisation of the nanoscale interfaces which are distributed within the dielectric. These results show that effective high dielectric constant hybrids using nanoscale inorganic dielectrics dispersed in a high permittivity polymer are promising for capacitors with enhanced energy storage but retain high power output capabilities.

Acknowledgements

This work was supported by Dyson Ltd. NM is also grateful to the Cambridge Commonwealth Trust for financial support and Prof. William Jones, Department of Chemistry, University of Cambridge for providing additional laboratory facilities. Gabriela

Schneider Rauber, Department of Chemistry, University of Cambridge is acknowledged for the support given for AFM cross section measurements.

References

1. Arico A P, Bruce P, Scrosati B, Tarascon J M and Schalkwijk W V 2005 *Nature Materials* **4** 366-77.
2. Yu G, Xie X, Pan L, Bao Z and Cui Y 2013 *Nano Energy* **2** 213-34.
3. Nelson J K and Fothergill J C 2004 *Nanotechnology* **15** 586-95.
4. Xie S H, Zhu B K, Wei X Z, Xu Z K and Xu Y Y 2005 *Composites:Part A* **36** 1152-57.
5. Zhou T, Zha J W, Cui R Y, Fan B H, Yuan J K and Dang Z M 2011 ACS *Appl. Mater. and interfaces* **3** 2184-88.
6. Kim P, Doss N M, Tillotson, J P, Hotchkiss P J, Pan M J, Marder S R, Li J, Calame J P and Perry J W 2009 *ACS Nano* **9** 2581-92.
7. Chiang C K and popielarz R 2002 *Ferroelectrics* **275** 1-9.
8. Culver S P, Beier, C W, Rafson J P and Brutchey R L 2014 *J. Appl. Polym. Sci.* **131** 40290-5.
9. Hong J I, Winberg P, Schadler L S and Siegel R W 2005 *Mat. Lett*. **59** 473-476.
10. Xu J and Wong C P 2005 *Appl. Phys. Lett.* **87** 082907-3.
11. Khastgir D, Maiti H S and Bandyopadhyay P C 1988 *Mat. Sci. and Eng.* **100** 245-53
12. Lewis T J 1994 *IEEE Trans*. **1**, 812-25.
13. Nelson J K, Fothergill J C and Dissado L A 2002 *Annu Rep IEEE Conf Electr Insul Dielectr Phen*: 295-98.
14. Chen F C, Chu C W, He J, Yang Y and Lin J L 2004 *Appl. Phys.Lett.* **85** 3295-3298.
15. Maliakal A, Katz H, Cotts P M, Subramoney S and Mirau P 2005 *J. Am. Chem. Soc.* **127** 14655-62.
16. Wei S, Mavinakuli P, Wang Q, Chen D, Asapu A and Mao Y 2011 *J. Electrochem. Soc.* **158** K205-12.
17. Prakash R R, Pandiarajan S, Venkatesh P and Kamaraj N 2011 *IEEE* ICETECT 46-49.
18. Li J, Seok S, Chu B, Dogan F, Zhang Q and Wang Q 2009 *Adv. Mater.* **21** 217-21.

19. Rekik H, Ghallabi Z, Royaud I, Arous M, Seytre G Boiteux G and Kallel A 2013 *Composites:Part B* **45** 1199-06.
20. Kim J, Lim S H and Kim Y S 2010 *J. Am. Chem. Soc*. **132** 14721-23.
21. Yu Y I, Yi M H and Ahn T 2012 *J. Ceram. Processing Res.* **13** s202-5.
22. Yen S P S, Lewis C R, Cygan P J and Jow T J 1992 *Power Sources Symposium IEEE 35th International Conference* 381-386.
23. Stefanov P, Shipochka M, Stefchev P, Raicheva Z, Lazarova V and Spassov L 2008 *Journal of Physics: Conference Series* **100** 012039-42.
24. Jonscher A K 1999 *J. Phys*. *D: Appl. Phys*. **32** R57-70.
25. Wang G, Moses D, Heeger A, Zhang H, Narasimhan M and Demaray 2004 *J. Appl. Phys*. **95** 316-22
26. Tanaka T, Kozako M and Fuse N and Ohki Y 2005 *Trans IEEE DEI* **12** 669-81.
27. Lewis T J 2005 *Trans IEEE DEI,* **11** 214-20.

Supplementary Information

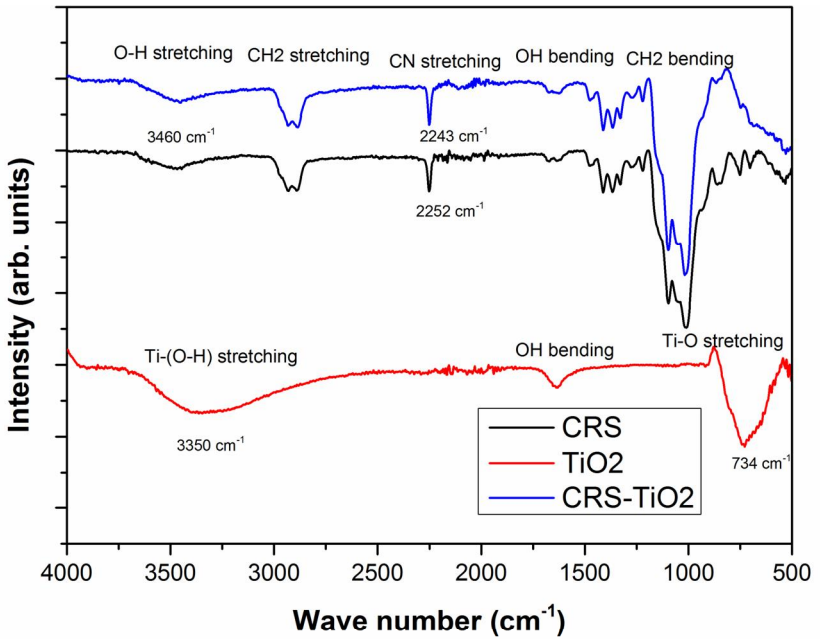

Figure S1 FTIR spectra of CRS, TiO_2 and CRS-TiO2 nanocomposite

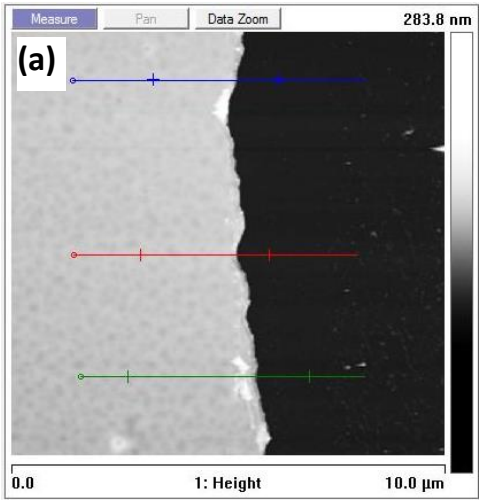

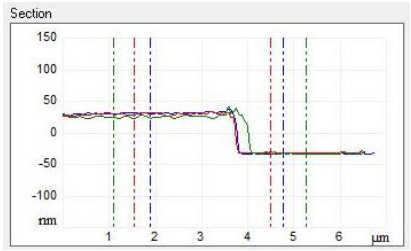

Pair	Vertical Dist.
0	-62.063...
1	-59.782...
2	-57.849...

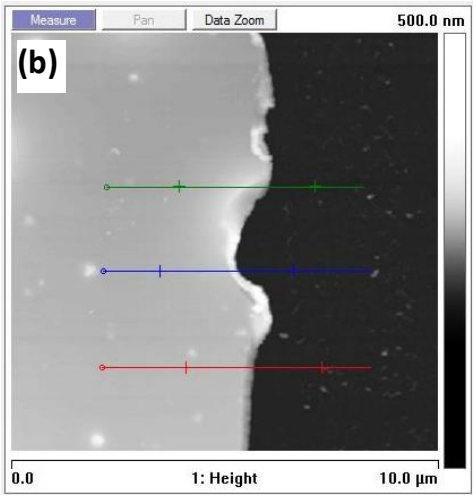

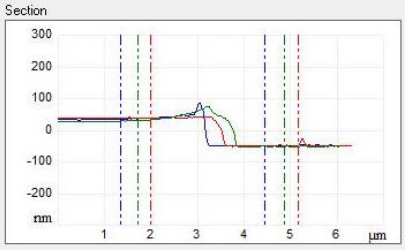

Pair	Vertical Dist.
0	-86.002...
1	-88.085...
2	-82.139...

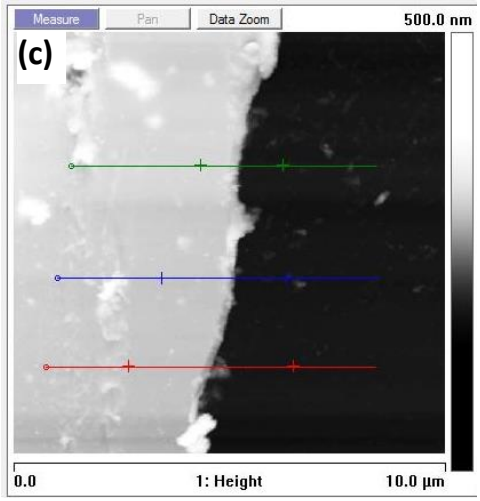

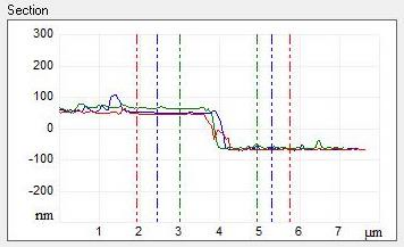

Pair	Vertical Dist.
0	-113.25...
1	-113.50...
2	-114.23...

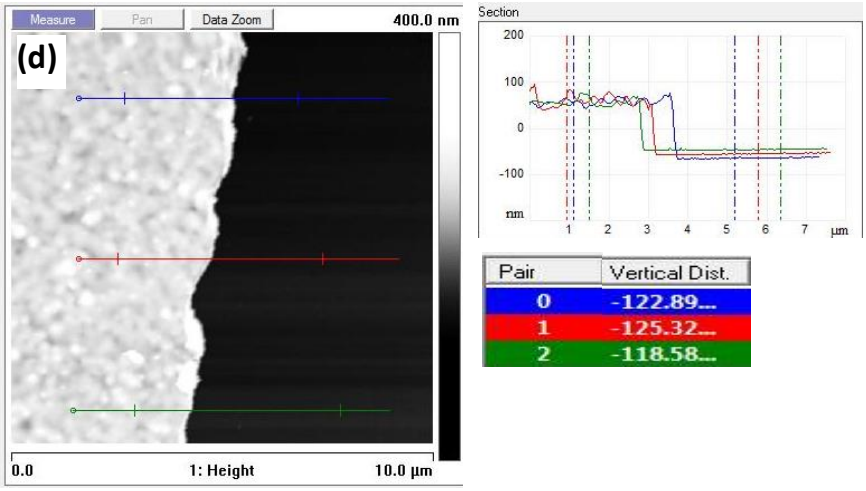

Figure S2 AFM surface scans and step profiles at film edges (a) CRS polymer (b) CRS-TiO2 10% (c) CRS-TiO2 10% (d) CRS-TiO_2 30% . The step profiles are used to determine film thickness (in nm).

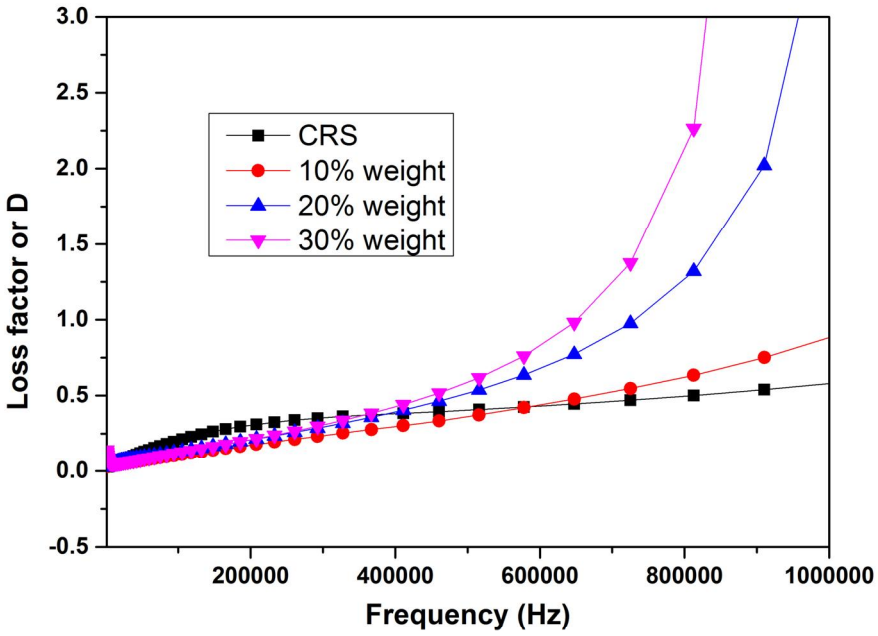

Figure S3 Lost factors for CRS-TiO2 nanocomposites with different TiO_2 loadings

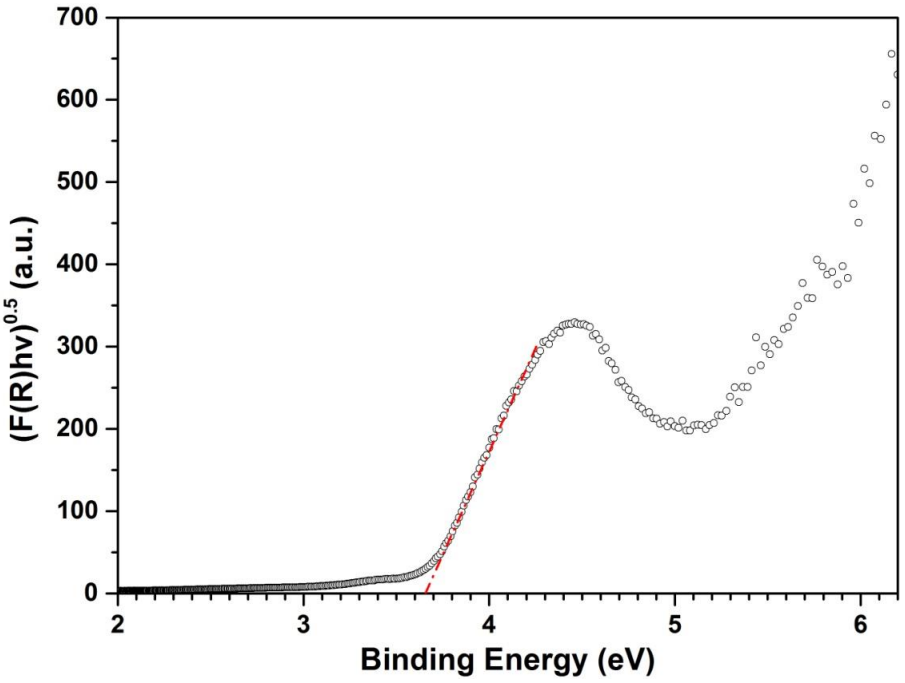

Figure S4 UV absorption spectra for CRS polymer; $(F(R)h\nu)^{\alpha}$ is proportional to absorption coefficient, where F(R) is the Kubelka-Munk function of reflection spectrum and exponent α equals to 0.5. As indicated in the inset the band gap is -3.66 eV.

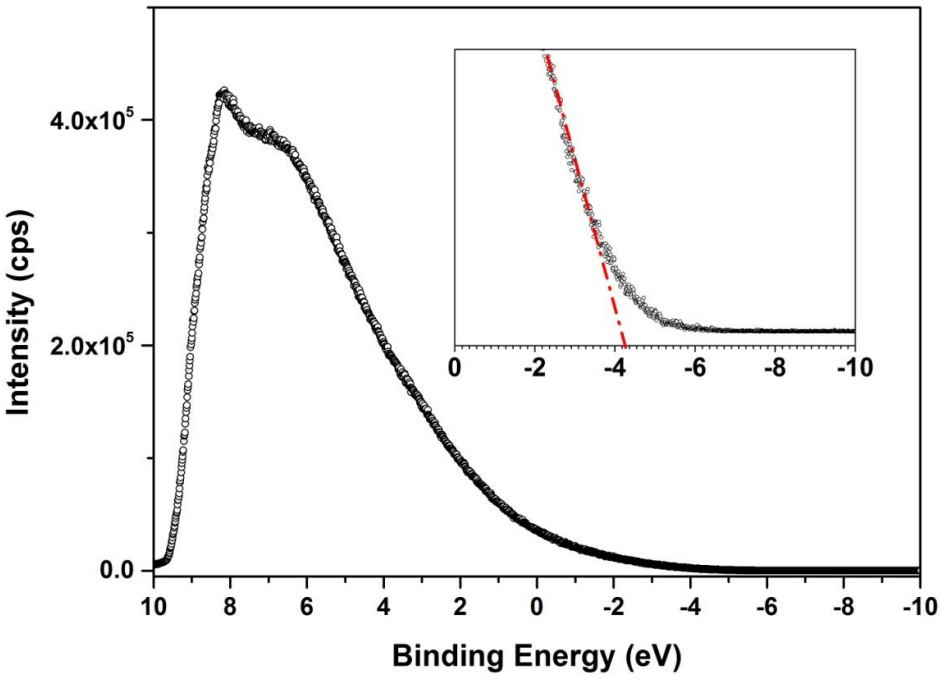

Figure S5 Ultra-violet Photoemission Spectra for CRS polymer and as indicated in the inset the Energy of Valance band is -4.15 eV in reference to vacuum level